Article

Cell Reports

Chemokine Signaling Enhances CD36 Responsiveness toward Oxidized Low-Density Lipoproteins and Accelerates Foam Cell Formation

Graphical Abstract

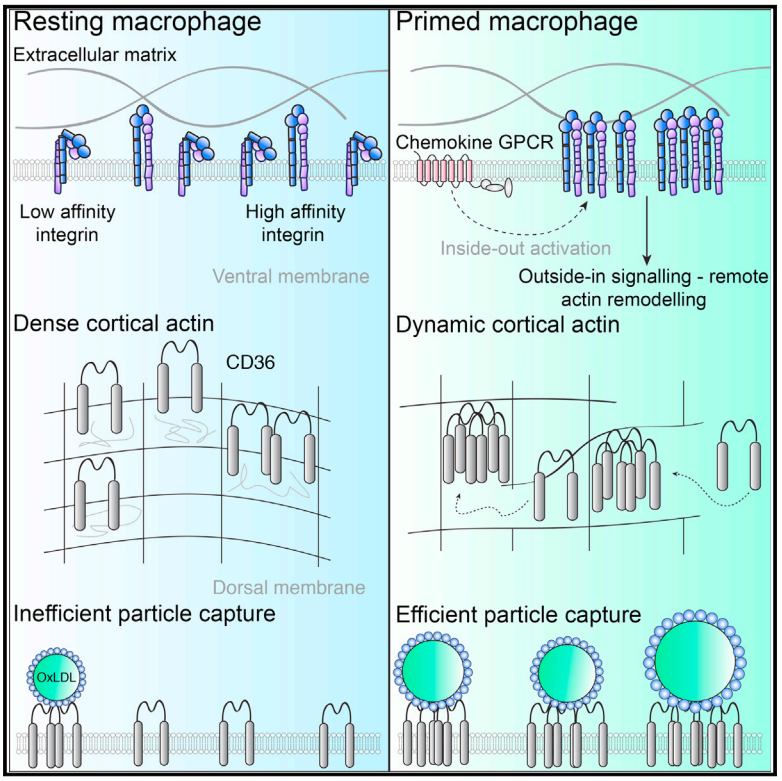

Highlights

- Chemokines enhance CD36 clustering by activating integrins
- Integrin signaling promotes CD36 clustering by altering cortical actin architecture
- Larger clusters of CD36 are primed for the engagement of multivalent oxLDL
- Prolonged exposure of macrophages to chemokines accelerates foam cell formation

Authors

Harikesh S. Wong, Valentin Jaumouillé, Spencer A. Freeman, ..., Amra Saric, Sergio Grinstein, Lisa A. Robinson

Correspondence

lisa.robinson@sickkids.ca

In Brief

The mechanisms that regulate the uptake of oxLDL by macrophages remain poorly defined. Wong et al. discovered a feedforward mechanism whereby the activation of integrins by chemokines remodels the cortical actin cytoskeleton to promote clustering of CD36, which subsequently enhances the engagement of oxLDL.

Wong et al., 2016, Cell Reports *14*, 2859–2871
March 29, 2016
http://dx.doi.org/10.1016/j.celrep.2016.02.071

CellPress

Cell Reports
Article

Chemokine Signaling Enhances CD36 Responsiveness toward Oxidized Low-Density Lipoproteins and Accelerates Foam Cell Formation

Harikesh S. Wong,[1,2] Valentin Jaumouillé,[1] Spencer A. Freeman,[1] Sasha A. Doodnauth,[1,3] Daniel Schlam,[1,2] Johnathan Canton,[1] Ilya M. Mukovozov,[1,2] Amra Saric,[4] Sergio Grinstein,[1,5] and Lisa A. Robinson[1,2,6,*]
[1]Program in Cell Biology, The Hospital for Sick Children Research Institute, Toronto, ON M5G 1X8, Canada
[2]Institute of Medical Science, University of Toronto, Toronto, ON M5S 2Z9, Canada
[3]Department of Medical Biophysics, University of Toronto, Toronto, ON M5S 2Z9, Canada
[4]Department of Chemistry and Biology, Ryerson University, Toronto, ON M5B 2K3, Canada
[5]Keenan Research Centre of the Li Ka Shing Knowledge Institute, St. Michael's Hospital, Toronto, ON M5B 1T8, Canada
[6]Department of Paediatrics, University of Toronto, Toronto, ON M5G 1X8, Canada
*Correspondence: lisa.robinson@sickkids.ca
http://dx.doi.org/10.1016/j.celrep.2016.02.071

SUMMARY

Excessive uptake of oxidized low-density lipoproteins (oxLDL) by macrophages is a fundamental characteristic of atherosclerosis. However, signals regulating the engagement of these ligands remain elusive. Using single-molecule imaging, we discovered a mechanism whereby chemokine signaling enhanced binding of oxLDL to the scavenger receptor, CD36. By activating the Rap1-GTPase, chemokines promoted integrin-mediated adhesion of macrophages to the substratum. As a result, cells exhibited pronounced remodeling of the cortical actin cytoskeleton that increased CD36 clustering. Remarkably, CD36 clusters formed predominantly within actin-poor regions of the cortex, and these regions were primed to engage oxLDL. In accordance with enhanced ligand engagement, prolonged exposure of macrophages to chemokines amplified the accumulation of esterified cholesterol, thereby accentuating the foam cell phenotype. These findings imply that the activation of integrins by chemokine signaling exerts feedforward control over receptor clustering and effectively alters the threshold for cells to engage ligands.

INTRODUCTION

Sterile inflammation is an inherent feature of atherosclerosis initiated by the accumulation of modified lipoproteins beneath the vascular wall. Among the reported modifications, oxidation of low-density lipoproteins is thought to be the most significant, promoting endothelial cell dysfunction and the recruitment of monocyte-derived macrophages to the vessel intima (Tabas et al., 2007; Williams and Tabas, 1999). While the internalization of oxLDL by recruited macrophages is initially deemed beneficial, excessive consumption results in the formation of cholesterol-rich foam cells, which, in turn, succumb to necrosis, release pro-inflammatory stimuli, and ultimately perpetuate a non-resolving, sterile inflammatory response (Seimon et al., 2010; Sheedy et al., 2013; Stewart et al., 2010). Why macrophages continually engulf oxLDL to their own detriment and to that of the surrounding microenvironment remains poorly understood.

In both human and murine macrophages, the engagement and internalization of oxLDL is primarily mediated by the class B scavenger receptor CD36 (Endemann et al., 1993; Febbraio et al., 2000; Kunjathoor et al., 2002; Nozaki et al., 1995). While many receptors are commonly assumed to exist as monomers in the plasma membrane, CD36 exists as multimers, which are metastable in the absence of ligand (Jaqaman et al., 2011). The pre-clustering of CD36 may prime macrophages to engage oxLDL, which is multivalent and can simultaneously engage multiple receptors (Jaqaman et al., 2011).

The ability of receptors to cluster is dictated by their lateral diffusion within the plane of the plasma membrane. However, it has become increasingly apparent that many barriers to diffusion exist, effectively limiting the extent of receptor clustering. In this regard, bulky transmembrane proteins can serve as molecular pickets anchored to underlying compartment boundaries, which are structured by the cortical actin cytoskeleton and impede the diffusion of mobile membrane proteins (Kusumi et al., 2005). To date, signals that modulate CD36 diffusion and clustering, and the resulting impact on the internalization of oxLDL, remain elusive.

During an inflammatory event, macrophages integrate multiple signals, generating context-dependent responses (Bezbradica et al., 2014; Freeman and Grinstein, 2014). Indeed, numerous studies using genetically modified mice suggest that the clearance of oxLDL during atherogenesis is a tunable process modulated by the cytokine milieu (Kleemann et al., 2008). Chemokines are among the initial cytokines encountered by a macrophage, guiding a continued influx of cells to the intima, and their effects persist throughout vascular inflammation. Although chemokines

are traditionally known for their role in orchestrating cell migration, they can influence immune cell function by several additional mechanisms (Zernecke and Weber, 2014). For instance, CX_3CL1, also known as fractalkine, serves as an anti-apoptotic, pro-survival signal for monocytes and macrophages (Landsman et al., 2009), while CXCL12 enhances macrophage phagocytosis of unopsonized *E. coli* as well as acetylated LDL (Ma et al., 2013). Activation of the Rap1 GTPase, which is a common signaling node triggered downstream of chemokine G protein-coupled receptors (GPCRs), can also enhance the phagocytic activity of macrophages toward certain ligands (Caron et al., 2000; Kim et al., 2012).

Given the accumulating evidence describing the function of chemokines beyond cell migration, and the significant contribution of chemokines to vascular disease (Zernecke and Weber, 2010), we investigated whether they could contribute to atherogenesis through additional mechanisms. Initially, we focused on the chemokine CX_3CL1, and later, generalized our findings to CCL2 and CXCL12. Our results demonstrate that by enhancing integrin activation and signaling, chemokines regulate the state of the cortical actin cytoskeleton, which in turn determines the extent of CD36 clustering. This mechanism controls the ability of macrophages to engage oxLDL and contributes to the formation of foam cells. These data suggest that modulation of receptor clustering by cytokines may serve as a generalized mechanism for fine-tuning ligand engagement and the progression of inflammation.

RESULTS

CX_3CL1 Signaling Enhances the Uptake of Oxidized Lipoproteins through CD36

We hypothesized that in addition to promoting migration and survival of monocytes/macrophages, CX_3CL1 could directly impact the uptake of oxLDL. To test this notion, oxLDL internalization was assessed in bone-marrow-derived macrophages (BMDMs) isolated from wild-type (WT) or CD36-deficient mice (Figures 1A and 1B). Following incubation with oxLDL and prior to fixation, cells were incubated briefly with trypsin, which cleaved exofacial receptor-ligand complexes, ensuring that only internalized oxLDL was quantified. As previously reported (Febbraio et al., 2000), CD36-deficient cells internalized approximately 60% less oxLDL when compared to WT counterparts (Figures 1A and 1B). The specificity of the oxLDL for CD36 was also confirmed through heterologous expression of CD36-GFP in HeLa cells (Figure S1A). When compared to non-transfected controls within the same field of view, CD36-GFP expressing cells bound 2.24-fold more oxLDL but bound a comparable amount of native LDL (Figures S1B and S1C). Interestingly, CD36-expressing cells also bound slightly more acetylated LDL compared to non-transfected controls (Figure S1C). In the presence of CX_3CL1, WT macrophages internalized 1.71-fold more oxLDL, an effect that was not observed in CD36-deficient cells (Figures 1A and 1B, $p < 0.05$ and $p < 0.0001$, respectively). Similar results were also observed in cultured murine RAW 264.7 macrophages using CD36 blocking antibodies (Figures S2A and S2B). These observations did not stem from global increases in endocytosis, as the uptake of transferrin, which occurs through clathrin-mediated endocytosis, was unaffected by CX_3CL1 (Figure S2C).

Enhanced internalization of oxLDL could result from increased receptor-ligand engagement. This possibility was investigated by incubating macrophages with oxLDL for 1 min. A brief exposure to trypsin cleaved >95% of receptor-ligand complexes, confirming that surface-bound rather than internalized oxLDL were being visualized (data not shown). As illustrated in Figures 1C and S2D, pre-incubation of BMDMs or RAW 264.7 macrophages with CX_3CL1 enhanced binding of oxLDL by 2.18- and 2.67-fold, respectively (Figures 1C and 1D, $p < 0.05$ versus control). These results were not due to non-specific effects of protein, or due to LPS contamination as macrophages deficient in the CX_3CL1 receptor, CX_3CR1, did not exhibit enhanced binding of oxLDL when exposed to the chemokine (Figure 1D). Furthermore, the increased binding was not due to enhanced surface expression of CD36 (Figure 1E). These data suggest that CX_3CL1 enhances the initial binding of oxLDL, likely by altering the kinetics of CD36-oxLDL interactions.

CX_3CL1 Increases the Lateral Diffusion and Clustering of CD36

CD36 was recently described to form metastable multimers in the absence of ligand (Jaqaman et al., 2011). Such pre-clustering may prime the cells for the engagement of multivalent ligand, by increasing the avidity of its interaction with receptors. Therefore, it was conceivable that exposing macrophages to CX_3CL1 might alter CD36 clustering and hence its ability to bind oxLDL. To assess this possibility, we imaged single receptors on the dorsal surface of human monocyte-derived macrophages (HMDMs) using anti-CD36 Fab fragments followed by secondary, Cy3-conjugated Fab fragments as previously described (Jaqaman et al., 2011). Since individual Cy3 fluorophores have defined fluorescence intensity, CD36 clustering was estimated based on the intensity of each feature. Of note, we determined that ≈85% of the secondary Fab fragments were conjugated to a single Cy3 (Figures S3A and S3B).

We proceeded to perform modal analysis of CD36 intensity histograms using the highest labeling density of Fab fragments that allowed us to resolve single features (Figure 2A). As previously described, multiple intensity modes were found in resting macrophages, confirming that CD36 exists as multimers (Figures 2A and 2C) (Jaqaman et al., 2011). Importantly, individual features photobleached in a stepwise fashion with a step size similar to both the mean of the first mode in the intensity histogram, and the intensity of a single Cy3 fluorophore, validating our ability to detect single molecules (Figures 2A and S3A–S3D). Following exposure to CX_3CL1, the fraction of CD36 features corresponding to one Cy3 fab fragment decreased from 0.72 ± 0.03 to 0.61 ± 0.02, while the fraction corresponding to two Cy3 increased from 0.24 ± 0.02 to 0.31 ± 0.02, and the fraction corresponding to three or more Cy3 increased from 0.04 ± 0.01 to 0.08 ± 0.01 (mean ± SEM, $p < 0.05$ for all comparisons, Figures 2A–2C). These results imply that CX_3CL1 increases CD36 clustering.

Increased CD36 clustering could be the result of increased lateral diffusion and subsequent receptor coalescence within the plane of the plasma membrane. To test this notion, we

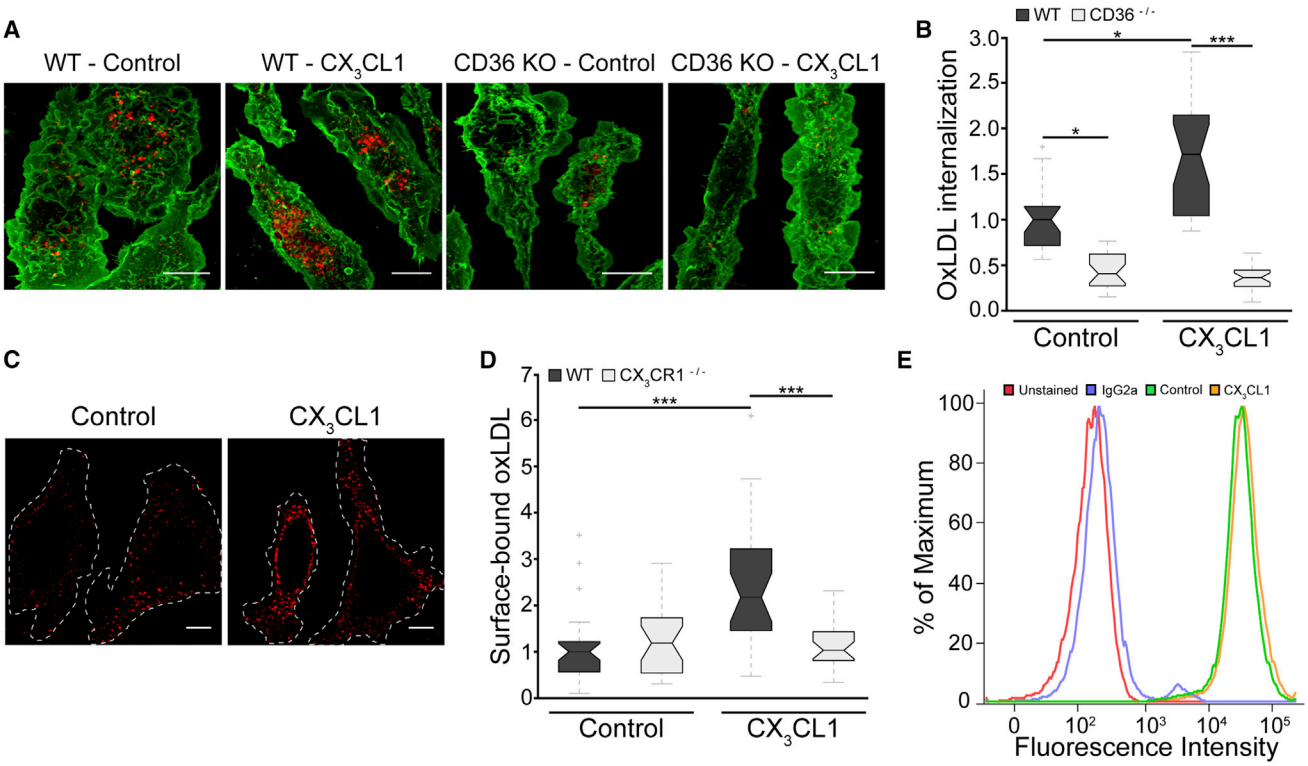

Figure 1. CX_3CL1 Increases CD36-Mediated Uptake of oxLDL

(A) Internalization of DiI oxLDL (red) was assessed for 20 min in WT or CD36$^{-/-}$ BMDMs treated with or without CX_3CL1. WGA-488 (green) was used to visualize the plasma membrane of individual cells. Representative extended focus projections obtained using spinning-disk confocal microscopy.

(B) Quantification of (A). The integrated fluorescence of DiI oxLDL was measured per cell (see Experimental Procedures). Data are from three independent experiments with BMDMs from three different mice. For each condition, 20–40 cells were quantified per experiment. Boxplots represent the pooled distribution of single cells, illustrating the median (central line), interquartile ranges (lower and upper regions of the box), inlier data points (gray dotted whiskers), and outlier data points (gray crosses).

(C) DiI oxLDL binding was assessed for 1 min in WT or $CX_3CR1^{-/-}$ BMDMs. Representative XY optical slices of WT BMDMs were obtained using spinning-disk confocal microscopy.

(D) Quantification of (C). DiI oxLDL fluorescence was quantified per cell as in (B). Data are from three independent experiments performed in BMDMs from two different mice. For each condition, 25–30 cells were quantified per experiment. Boxplots are as in (B).

(E) Surface expression of CD36 control or CX_3CL1-treated RAW 264.7 macrophages assessed by flow cytometry. Representative histogram illustrating the fluorescence distribution of single cells (n = 3).

For (A) and (C), scale bars, 10 μm. For (B) and (D), *$p < 0.05$, ***$p < 0.0001$ were determined by the Kruskal-Wallis test using Dunn's multiple comparisons test. See also Figure S1.

performed single-molecule tracking of CD36 using quantum dots (Qdots) as described by Jaqaman et al. (2008, 2011) (see Experimental Procedures). Previously, CD36 diffusion was classified using two approaches. First, individual trajectories were characterized as linear or isotropic. Second, these same trajectories were subjected to moment scaling spectrum (MSS) analysis, which classifies motion as either confined (subdiffusive) or free (Jaqaman et al., 2008, 2011). While all components of the analysis are documented in Figure S3E, for simplicity the results hereafter are classified as confined and free motion, irrespective of linearity. As shown in Figures 2D and 2E, exposing macrophages to CX_3CL1 enhanced the diffusion of CD36, decreasing confined motion from 59% ± 3% to 41% ± 2%, while increasing free motion from 41% ± 3% to 59% ± 2% (mean ± SEM, $p < 0.0001$ for each comparison). The overall diffusion coefficient of CD36 also increased from 0.024 ± 0.002 $\mu m^2/s$ to 0.035 ± 0.002 $\mu m^2/s$ (mean ± SEM, $p < 0.05$, Figure 2F). Taken together, these results suggest that CX_3CL1 increases the ability of CD36 to form transient clusters by increasing the lateral diffusion of the receptor.

CX_3CL1 Dynamizes the Actin Cytoskeleton, Creating Zones that Facilitate CD36 Clustering

The lateral diffusion and clustering of CD36, as well as other immunoreceptors, is governed in part by the cortical actin cytoskeleton (Andrews et al., 2008; Freeman et al., 2015; Jaqaman et al., 2011; Jaumouillé et al., 2014). Because CX_3CL1 was reported to alter actin cytoskeletal dynamics in macrophages (Gevrey et al., 2005; Park and Cox, 2011), we considered whether it increased CD36 clustering and diffusion by remodeling the cytoskeleton. Similar to previous studies (Gevrey et al., 2005), CX_3CL1 induced the formation of actin-driven ruffles (Figure 3A). In addition to

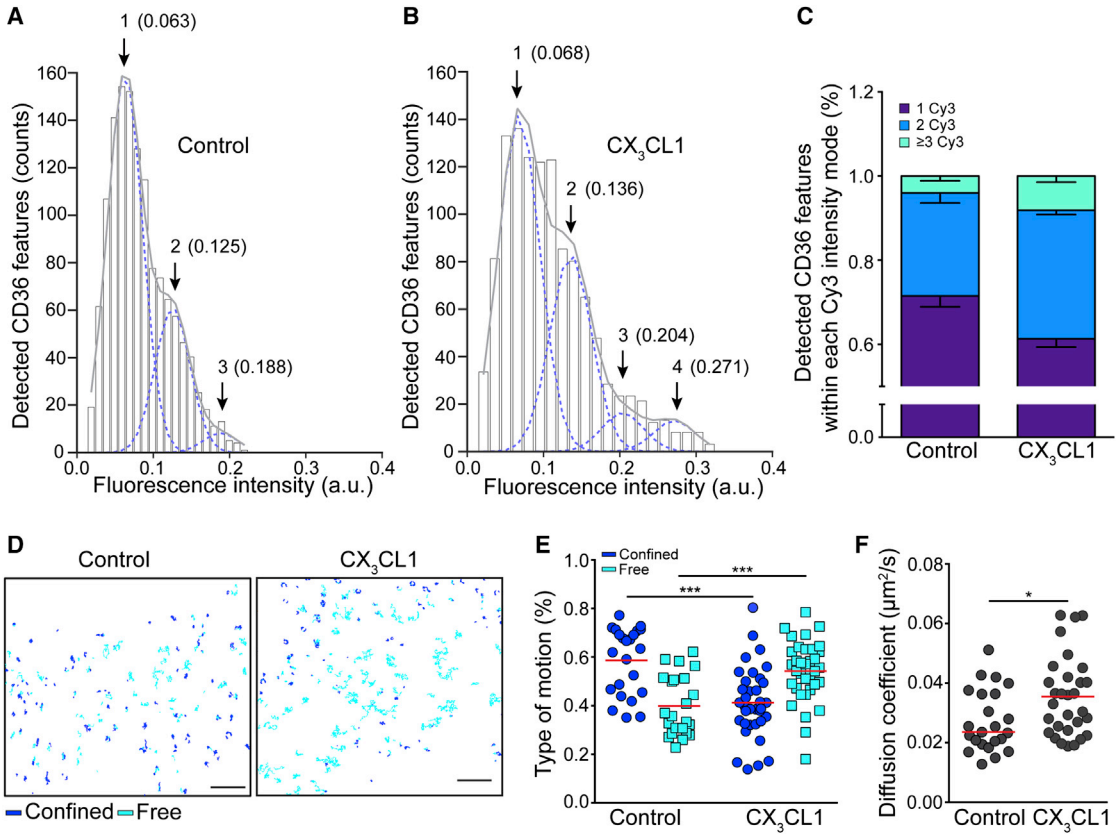

Figure 2. CX_3CL1 Increases the Lateral Diffusion and Clustering of CD36

(A and B) Control (A) and CX_3CL1-treated (B) HMDMs. Representative fluorescence intensity histogram of cell-surface CD36 molecules detected using Cy3-conjugated Fabs decomposed into individual intensity modes (dotted blue lines, individual modes; solid gray lines, sum of all modes). Arrows indicate each mode center; numbers represent the fluorescence intensity of each mode center.

(C) CD36 clustering determined using the modal analysis in (A) and (B). Data are from three independent experiments, each with eight to 15 cells per condition.

(D) Single-molecule tracking of cell-surface CD36 in control or CX_3CL1-treated HMDMs. CD36 molecules were detected using Qdots and recorded at 33 Hz for 10 s. Motion was determined using MSS analysis. Representative CD36 trajectories are shown (blue, confined motion; cyan, free motion). Scale bars, 4 μm.

(E) Fraction of CD36 molecules undergoing confined and free motion with and without CX_3CL1. ***$p < 0.0001$ was determined by unpaired, two-tailed t test.

(F) Median diffusion coefficients for all particles (irrespective of motion type) with and without CX_3CL1.

*$p < 0.05$ was determined by unpaired, two-tailed t test. For (E) and (F), individual dots correspond to single cells pooled from three independent experiments, each with eight to 12 cells. Horizontal lines represent the means of the pooled data. See also Figure S2.

ruffling, two additional phenomena were observed. First, compared to resting macrophages, CX_3CL1 significantly reduced the amount of cortical F-actin at the dorsal cell surface, resulting in a decrease in the dorsal to ventral F-actin ratio (Figures 3B and 3C). Of note, the decrease in dorsal F-actin coincided with the appearance of podosome structures on the ventral surface (Figure 3B). Second, exposure to CX_3CL1 introduced pronounced heterogeneity in the distribution of dorsal cortical F-actin, promoting the appearance of actin-poor regions adjacent to actin-rich ruffles (Figures 3B and 3D). This was in sharp contrast to resting macrophages, which exhibited relatively thick, homogenous cortical F-actin at the dorsal surface (Figures 3B and 3C). Despite these effects on cytoskeletal rearrangement, CX_3CL1 did not alter the total F-actin content per cell (Figure 3E).

Ruffling is thought to be critical for the capture of immunoglobulin G (IgG)-opsonized targets by innate immune cells (Flannagan et al., 2010). It is therefore conceivable that ruffles also aid in the capture of oxLDL. This hypothesis was initially investigated by immunostaining for CD36, followed by structured illumination microscopy (SIM), which enabled us to assess the distribution of the receptor with respect to the ruffles beyond the resolution of conventional, diffraction-limited microscopy. Remarkably, CD36 clusters were predominantly excluded from F-actin ruffles, residing instead in adjacent F-actin-poor zones of the cortex (Figures 3F, 3G, S4A, and S4C). Furthermore, clusters of CD36 in actin-poor zones were 2.6 ± 0.4-fold larger than those in actin-rich regions (Figure 3G; mean ± SEM, $p < 0.001$). By contrast, FcγIIa receptors, which bind IgG opsonized targets, were found homogenously distributed throughout ruffles and the dorsal cortex (Figure S4B), suggesting that the uneven distribution of CD36 was not an artifact of the SIM deconvolution process. Most importantly, larger oxLDL particles preferentially bound to the F-actin-depleted zones in which CD36 clusters

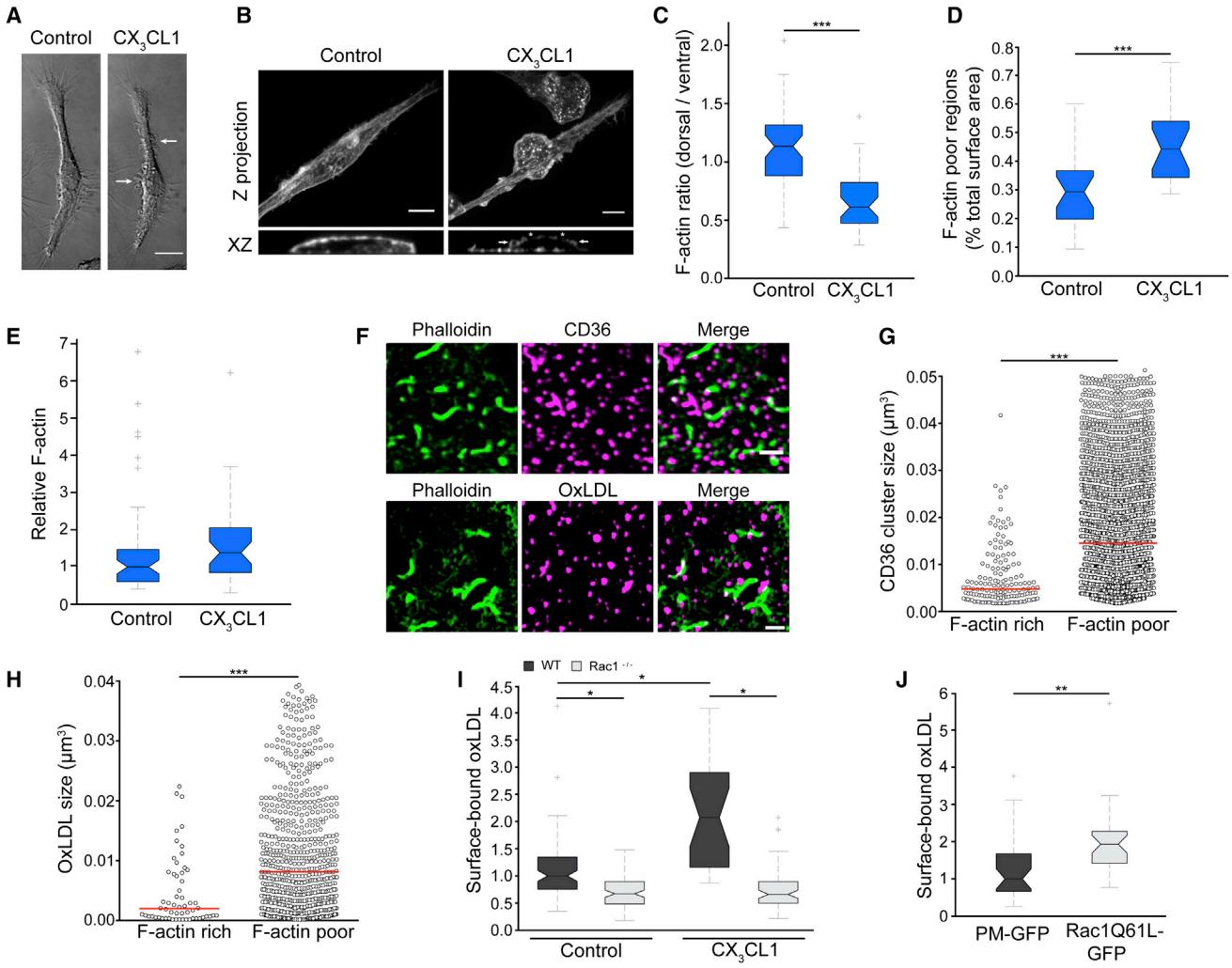

Figure 3. CX_3CL1 Dynamizes the Actin Cytoskeleton, Creating Zones that Facilitate CD36 Clustering

(A) Representative DIC stills from a time-lapsed video of the same HMDM before and after treatment with CX_3CL1. Arrows highlight peripheral and dorsal ruffles.

(B) F-actin distribution in HMDMs with and without CX_3CL1 visualized with phalloidin-488. Representative extended focus z projections (top) and corresponding XZ optical slices (bottom) obtained using spinning-disk confocal microscopy. Arrows highlight ruffles and asterisks highlight adjacent, F-actin poor regions.

(C) Quantification of the dorsal to ventral F-actin ratio per cell based on phalloidin-488 fluorescence intensity. ***$p < 0.0001$ was determined by the Kolmogorov-Smirnov test.

(D) Quantification of the F-actin poor regions per cell as a percentage of total surface area based on phalloidin-488 fluorescence intensity. ***$p < 0.0001$ was determined by the Kolmogorov-Smirnov test.

(E) Quantification of total F-actin based on the integrated phalloidin-488 intensity per cell. For (C)–(E), data are from three independent experiments, each with ten to 20 cells. Boxplots are as in Figure 1.

(F) Cell-surface CD36 (top panel, clone MF3) and Alexa-647-conjugted oxLDL (bottom panel) distribution was assessed with respect to F-actin in BMDMs. Representative XY optical slices obtained using SIM. Scale bars, 1 µm.

(G and H) Quantification of (F). Distribution of CD36 cluster size and oxLDL particle size within actin-rich and actin-poor regions measured throughout an entire cell in 3D. Each dot corresponds to an individual CD36 cluster or oxLDL from a single, representative cell. Red lines represent median particle size. Three independent experiments were performed, each with five cells. ***$p < 0.0001$ was determined by the Kolmogorov-Smirnov test.

(I) Dil oxLDL binding was performed as in Figure 1C in BMDMs derived from WT or Rac1-deficient (Rac $1^{-/-}$) mice. Data are from three independent experiments, each with 28–40 cells, and are normalized to the WT control. Boxplots are as in Figure 1. *$p < 0.05$ was determined by the Kruskal-Wallis test using Dunn's multiple comparisons test.

(J) HMDMs expressing a generic plasma membrane marker (PM-GFP) or constitutively active Rac1 (RacQ61L-GFP). Quantification of oxLDL binding was performed as in (G).

Data are from three independent experiments, each with eight to 12 cells. Boxplots are as in (C)–(E) and (G). **$p < 0.01$ was determined by the Kolmogorov-Smirnov test. See also Figure S3.

resided (Figures 3F, 3H, and S4D). It should be noted that uncontrolled disruption of F-actin was not sufficient to increase binding of oxLDL as exposing macrophages to a low concentration of latrunculin B (500 nM for 4 min) increased CD36 diffusion, yet had little effect on oxLDL engagement (Figures S3F and S3G; data not shown). Therefore, a dynamic balance between ruffling and the creation of zones poor in F-actin is required to enhance oxLDL binding. Collectively, these data suggest that CX_3CL1 creates actin-poor zones that promote CD36 receptor coalescence.

We proceeded to confirm that CX_3CL1-induced cytoskeletal remodeling was required for enhanced oxLDL binding. Initially, BMDMs were isolated from either WT mice, or mice deficient in Rac1 ($Rac1^{-/-}$), a critical mediator of cytoskeletal dynamics that has previously been implicated in CX_3CL1-induced ruffling, as well as cytokine-induced ruffling in general (Park and Cox, 2011; Ridley et al., 1992; Wells et al., 2004). In response to CX_3CL1, WT macrophages bound twice as much oxLDL compared to untreated controls ($p < 0.05$ versus WT control) (Figure 3I). However, this effect was not observed in the $Rac1^{-/-}$ macrophages ($p < 0.05$). These results were verified by transfecting HMDMs with a plasmid encoding a constitutively active form of Rac1 (Rac1Q61L-GFP), generating a dynamic actin cortex comprising oversized ruffles and adjacent F-actin-poor zones (Figures S4E and S4F). Expression of Rac1Q61L-GFP increased binding of oxLDL by 1.93-fold compared to cells expressing a generic plasma membrane marker (PM-GFP) as a control ($p < 0.001$) (Figure 3J). Therefore, the effects of CX_3CL1 on oxLDL engagement are mediated by cytoskeletal remodeling.

CX_3CL1 Increases oxLDL Binding by Activating Integrins

We next questioned the mechanism by which CX_3CL1 altered the cytoskeleton. In macrophages, integrin-mediated adhesion and subsequent outside-in signaling can dictate the organization of the actin cytoskeleton, in part by regulating Rho GTPases such as Rac1 (Abram and Lowell, 2009; del Pozo et al., 2004; Jaumouillé et al., 2014; Okigaki et al., 2003). Since CX_3CL1 caused a significant increase in the appearance of podosomes (Figures 3B and 4A), which are integrin-rich structures implicated in cell adhesion, and because many chemokines have been reported to promote integrin activation (Abram and Lowell, 2009; Murphy and Courtneidge, 2011), we tested whether integrin-mediated adhesion influenced oxLDL binding. To this end, we employed specific β1 and β2 integrin blocking antibodies and found that they significantly limited CX_3CL1-induced actin responses and the binding of oxLDL (Figures 4B and 4C). EDTA was next used to inhibit integrins and lift macrophages into suspension. Following the removal of EDTA by washing, cells were re-suspended in medium containing calcium, incubated with chemokine, and assessed for their ability to engage oxLDL. As shown in Figure 4D, exposing suspended macrophages to CX_3CL1 had little effect on the engagement of oxLDL. Therefore, CX_3CL1 enhances oxLDL binding in adherent cells only, seemingly by remodeling the cytoskeleton following integrin engagement.

We proceeded to confirm that CX_3CL1 in fact promoted integrin-mediated adhesion. Initially, cell spreading on integrin ligands was assessed. HMDMs were lifted into suspension and re-plated onto the integrin ligand, fibronectin, revealing that CX_3CL1 increased the spreading area of cells from 510 μm^2 (interquartile range [IQR] = 219–949 μm^2) to 1116 μm^2 (IQR = 783.6–2180 μm^2) ($p < 0.0001$) (Figure 4E). Furthermore, CX_3CL1 doubled the number of adherent cells per field of view (Figure S5A). Increased adhesion could be the result of inside-out integrin activation, which involves activation of the Rap1 GTPase. (Abram and Lowell, 2009). Consistent with this notion, we found that CX_3CL1 increased the amount of active Rap1 (Rap1-GTP) in macrophages by 74% ($p < 0.0001$) compared to untreated controls (Figure 4F). Additionally, treatment with CX_3CL1 significantly increased binding of the MEM-148 monoclonal antibody, which recognizes the high affinity, β2 integrin conformation (Figure S5B).

The role of Rap1 in oxLDL binding was next probed by transfecting RAW 264.7 macrophages with a plasmid encoding Rap1-GapII, which hydrolyzes active Rap1-GTP to the inactive form, Rap1-GDP. As illustrated in Figures 4G and 4H, cells expressing Rap1GapII did not respond to CX_3CL1 ($p < 0.0001$) compared to untransfected controls in the same field of view, and even bound less oxLDL under basal conditions ($p < 0.05$). Conversely, expressing a constitutively active form of Rap1 (Rap1V12) enhanced binding of oxLDL 1.7-fold (IQR = 1.35–2.20) ($p < 0.0001$ versus control) (Figure 4I).

Following inside-out activation, integrins more readily engage their ligands, such as extracellular matrix (ECM) proteins, and transduce outside-in signals that alter actin cytoskeletal architecture. These signals can remodel actin both locally and remotely, likely accounting for the effect of CX_3CL1 on CD36 clustering and oxLDL binding at the dorsal cell surface. In order to transmit most outside-in signals, integrins must anchor the underlying actin cytoskeleton through linkers such as talin and vinculin (Abram and Lowell, 2009). While macrophages transfected with WT talin (TalinWT-GFP) responded normally to CX_3CL1 and bound more oxLDL, those transfected with TalinHD, which serves as a dominant negative for the endogenous protein, did not ($p < 0.0001$ versus Talin-WT + CX_3CL1, Figures 4J and 4K). In fact, cells expressing TalinHD bound ~40% less oxLDL even under basal conditions when compared to cells expressing TalinWT ($p < 0.05$; Figure 4K). Taken together, these observations are most consistent with a model whereby CX_3CL1 activates the Rap1 GTPase and promotes integrin-mediated adhesion. The resulting outside-in integrin signals then act at remote sites of the cell, remodeling cortical actin at the dorsal surface, which, in turn, increases CD36 clustering and subsequent binding of oxLDL.

CD36 Clustering Is Regulated by Chemokine Signaling

The conserved activation of the Rap1 GTPase and integrins downstream of chemokine GPCRs suggests that the effect of CX_3CL1 on CD36 clustering may be a generalized phenomenon induced by numerous chemokines. To explore this possibility, we selected two additional, structurally distinct chemokines that can activate Rap1 and assessed their effects on CD36 clustering and oxLDL binding (Katagiri et al., 2003; Yi et al., 2012). Among the possible candidates, we chose CCL2, which has previously been implicated in potentiating the severity of atherosclerosis, and CXCL12, which has been implicated in promoting

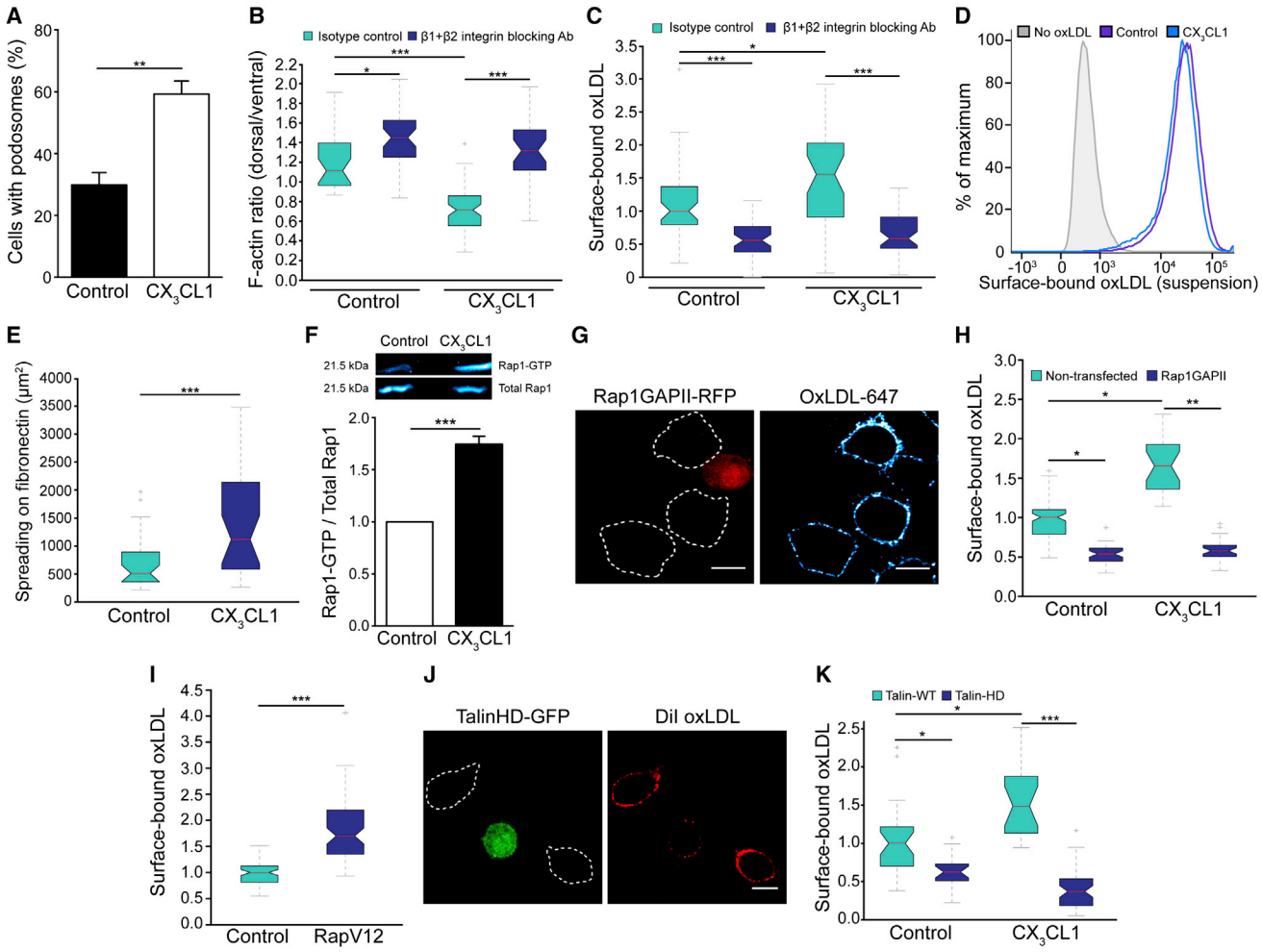

Figure 4. CX_3CL1 Increases oxLDL Binding by Activating Integrins

(A) Quantification of the percentage of HMDMs with visible podosomes assessed by phalloidin-488 staining. Data are mean ± SEM from three independent experiments, each with 15–30 cells quantified. **$p < 0.001$ was determined by unpaired two-tailed t test.

(B) HMDMs were pre-incubated with an isotype control, or β1 and β2 integrin blocking Abs before being exposed to CX_3CL1. Quantification of the dorsal to ventral F-actin ratio as in Figure 3C.

(C) HMDMs treated as in (B). Binding of DiI oxLDL was assessed as in Figure 1C. For (B) and (C), data are from three independent experiments, each with ten to 20 cells quantified. Boxplots are as in Figure 1B. *$p < 0.05$, ***$p < 0.0001$ were determined by the Kruskal-Wallis test using Dunn's multiple comparisons test.

(D) Binding of Alexa-647-conjugted oxLDL to RAW 264.7 macrophages in suspension pre-treated with or without CX_3CL1. Representative histogram demonstrating the fluorescence distribution of single cells obtained using flow cytometry (n = 3).

(E) HMDMs were laid onto fibronectin-coated substrates for 10 min. Quantification of the spreading area in cells pre-treated with or without CX_3CL1. ***$p < 0.0001$ was determined by the Kolmogorov-Smirnov test.

(F) Quantification of Rap1-GTP in RAW 264.7 macrophages treated with CX_3CL1 (1 min) by biochemical pull-down using RalGDS-GST. Ratio of Rap1-GTP to total Rap1 was normalized to control conditions. Representative immunoblot (top panel). Data are mean ± SEM from three independent experiments. ***$p < 0.0001$ was determined by unpaired two-tailed t test.

(G) RAW 264.7 macrophages expressing Rap1GAPII-RFP. Alexa-647-conjugated oxLDL binding was assessed as in Figure 1C. Representative XY optical slices of CX_3CL1-treated macrophages obtained using spinning-disk confocal microscopy. Scale bar, 10 μm.

(H) Quantification of (E) as in Figure 1D. Only transfected and non-transfected cells within the same field of view were compared. Data are from three independent experiments, each with ten to 12 cells, and normalized to non-transfected controls.

(I) RAW 264.7 macrophages expressing constitutively active, Rap1V12-RFP. Alexa-647-conjugated oxLDL binding was assessed and quantified as in (E) and (F).

(J) RAW 264.7 macrophages expressing TalinWT-GFP or dominant-negative talin (TalinHD-GFP). DiI oxLDL binding was assessed as in (E). Representative XY optical slices of CX_3CL1-treated macrophages were obtained using spinning-disk confocal microscopy. Scale bar, 10 μm.

(K) Quantification of (D).

Data are from three independent experiments, each with ten to 15 cells, and normalized to control, TalinWT-GFP. Boxplots are as in Figure 1B. *$p < 0.05$, ***$p < 0.0001$ were determined by the Kruskal-Wallis test using Dunn's multiple comparisons test. See also Figure S4.

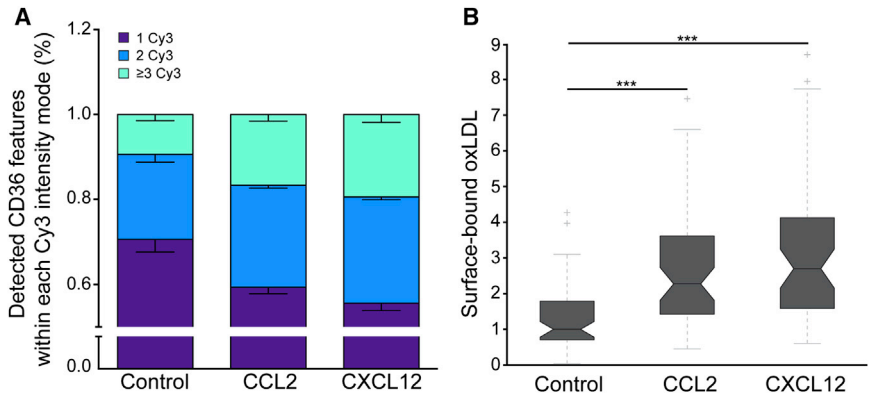

Figure 5. Chemokine Signaling Enhances CD36 Clustering and the Binding of oxLDL

(A) HMDMs were treated with CCL2 or CXCL12 and CD36 clustering was assessed as in Figure 2C. Data are from three independent experiments, each with eight to ten cells quantified.

(B) HMDMs were treated as in (A), and oxLDL binding was assessed as in Figure 1C. Data are from three independent experiments, each with 18–20 cells quantified. ***$p < 0.0001$ was determined by the Kolmogorov-Smirnov test.

macrophage phagocytosis (Boring et al., 1998; Ma et al., 2013). As illustrated in Figure 5A, both CCL2 and CXCL12 significantly decreased the fraction of CD36 features corresponding to one Cy3 fab fragment while concomitantly increasing the fraction of CD36 features corresponding to two and three or more Cy3 fab fragments. In support of enhanced receptor clustering, we also found that CCL2 and CXCL12 increased the binding of oxLDL by 2.27- (IQR = 1.42–3.64) and 2.7-fold (IQR = 1.58–4.12), respectively (Figure 5B). These data demonstrate that, in general, chemokine-induced activation of integrins enhances CD36 clustering and the binding of oxLDL.

Integrins Control the Threshold of Responsiveness for CD36

To assess more directly the role of integrin signaling in CD36 responsiveness, we developed a model system where the degree of integrin engagement could be tightly controlled. Our approach entailed lifting HMDMs and re-plating them onto coverslips saturated with 5% BSA, which limits integrin-mediated adhesion, or coverslips with defined integrin ligands (i.e., fibronectin or collagen). When laid onto BSA, cells exhibited a round morphology, reflecting impaired cell spreading (Figure 6A). Further analysis of the resting cytoskeleton structure revealed that limiting integrin engagement led to the development of an extremely dense, homogenous actin cortex (Figure 6A). In contrast, laying cells onto either fibronectin or collagen resulted in a dynamic actin cortex, with large ruffles and adjacent actin-depleted zones. Engaging integrins also led to the marked depletion of cortical F-actin from the dorsal membrane (Figure 6A). In line with these observations, the dorsal to ventral F-actin ratio decreased from 1.02 (IQR = 0.75–1.27) on BSA to 0.61 (IQR = 0.44–0.74) on fibronectin and 0.48 (IQR = 0.37–0.62) on collagen ($p < 0.0001$ fibronectin or collagen versus BSA) (Figure 6B). Moreover, the amount of F-actin-poor zones as a percentage of total surface area increased drastically from 0.15 (IQR = 0.11–0.25) on BSA to 0.73 (IQR = 0.64–0.79) on fibronectin and 0.55 (IQR = 0.41–0.61) on collagen ($p < 0.0001$ fibronectin or collagen versus BSA) (Figure 6C). The observed results were not due to changes in total cellular F-actin content but rather reflected a redistribution of F-actin (Figure 6D). Thus, integrin signaling regulates the state of the cortical actin cytoskeleton both at the dorsal and ventral membrane of macrophages.

If integrin-mediated adhesion regulates the resting cytoskeleton, it is conceivable that a feedforward mechanism exists between the degree of outside-in integrin signaling and CD36 responsiveness. In accordance with this concept, modal analysis of intensity histograms, as in Figure 2, revealed that CD36 cluster size increased significantly on integrin ligands when compared to BSA (Figure 6E). Furthermore, single-molecule tracking experiments demonstrated that CD36 was much less confined and moved with significantly faster diffusion coefficients on integrin ligands, accounting for increased receptor clustering (Figures 6F and 6G). These results suggest that integrin signaling may sensitize CD36 to engage multivalent oxLDL. This hypothesis was tested by measuring the engagement of oxLDL in macrophages laid onto BSA, fibronectin, or collagen. Strikingly, cells on fibronectin or collagen bound 3.2- and 2.1-fold more oxLDL, respectively, compared to cells on BSA ($p < 0.0001$ fibronectin versus BSA, $p < 0.001$ collagen versus BSA) (Figure 6H). To further verify these results, outside-in integrin signaling was artificially induced using cross-linking antibodies. As Figure 6I illustrates, cross-linking β1 or β2 integrins with monoclonal antibodies followed by Fab2 increased CD36 cluster size as well as binding of oxLDL by 2.5- and 2.3-fold, respectively ($p < 0.0001$ versus control) (Figures S5C and S5D; Figure 6I). Note that caution was taken to block Fc receptors prior to the addition of integrin antibodies to avoid confounding signaling. Overall, these data demonstrate that, by controlling cytoskeletal architecture, integrins set the threshold of responsiveness for CD36, thereby regulating the engagement of oxLDL.

Chemokines Accelerate Macrophage Foam Cell Formation

The results hitherto demonstrate that increased integrin engagement induced by chemokine signaling or by physical cross-linking sensitizes CD36 to engage ligand. Functionally, enhanced responsiveness toward oxLDL could promote the excessive accumulation of cholesterol and, thus, the formation of macrophage-derived foam cells that drive sterile inflammation. Macrophages esterify non-essential cholesterol for storage in specialized organelles called lipid droplets. To assess the effect of the chemokines on foam cells, lipid droplet formation was assessed using the non-polar probe BODIPY in macrophages incubated with high concentrations of oxLDL. In keeping with enhanced ligand engagement, CX_3CL1, CCL2, and CXCL12

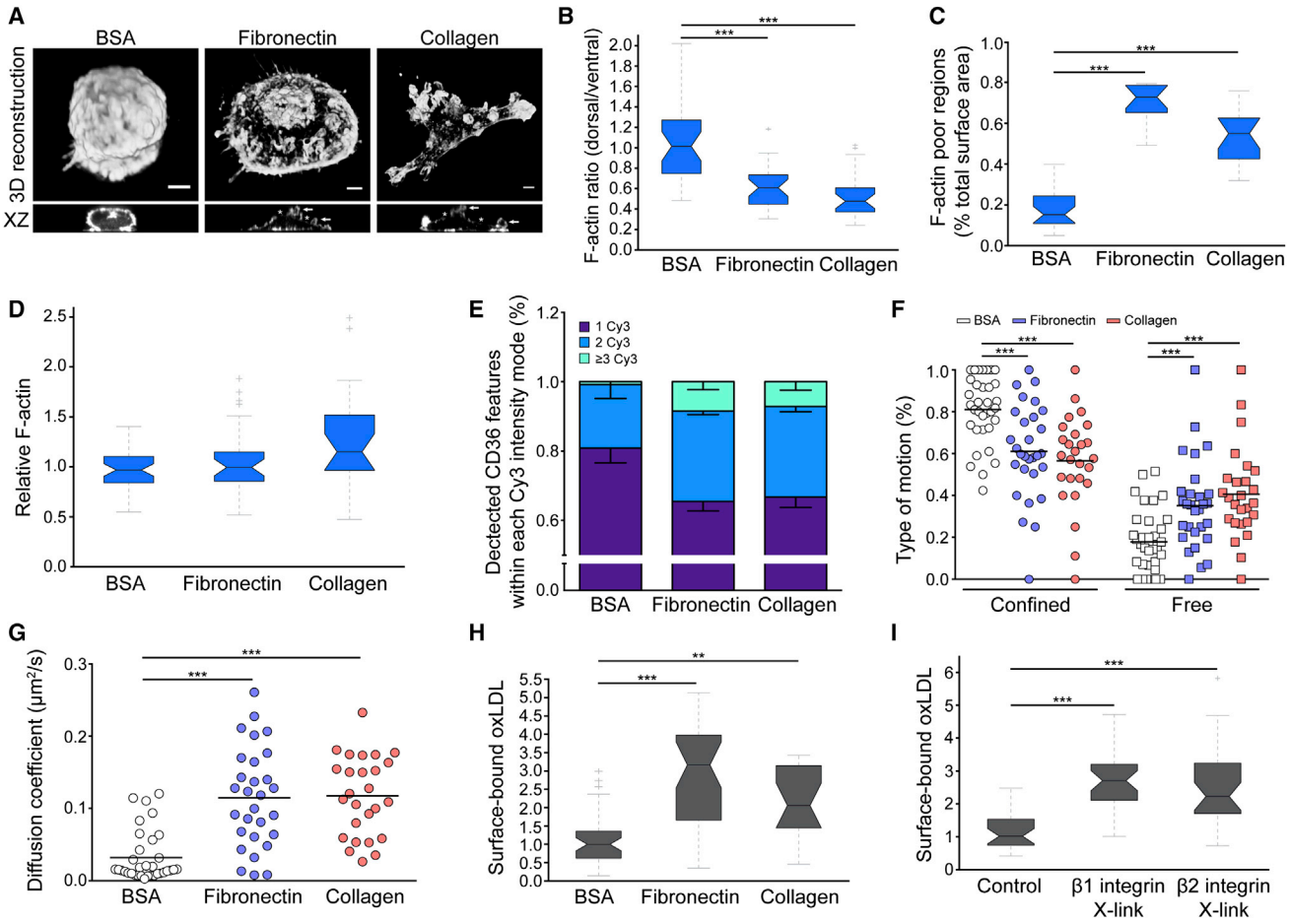

Figure 6. Integrins Control the Threshold of Responsiveness for CD36

(A) HMDMs were dropped onto 5% BSA, fibronectin, or collagen-coated substrates for 45 min and stained with phalloidin-488. Representative 3D opacity reconstructions and corresponding XZ optical slices were obtained using spinning-disk confocal microscopy. Arrows highlight ruffles and asterisks highlight adjacent, F-actin depleted regions. Scale bars, 10 μm.

(B–D) Quantification of the dorsal to ventral F-actin ratio, F-actin depleted regions, and relative F-actin as in Figures 3D–3F. Data are from three independent experiments, each with ten to 15 cells. Boxplots are as in Figure 1B. ***$p < 0.0001$ was determined by the Kolmogorov-Smirnov test.

(E) CD36 clustering analysis in HMDMs laid on different substrates determined as in Figures 2A–2C. Data are from three independent experiments, each with five to ten cells per condition.

(F and G) Cells were laid onto different substrates (F) as in (A) and (E) and labeled for single-molecule tracking as in Figure 2D. Fraction of CD36 molecules undergoing confined and free motion and (G) median diffusion coefficients are shown. Data are from three independent experiments, each with eight to ten cells. Dot plots are as in Figure 2.

(H) Macrophages were laid onto different substrates as in (A), and Alexa-647-conjugated oxLDL binding was assessed and quantified as in Figure 4. ***$p < 0.0001$,**$p < 0.001$ were determined by the Kolmogorov-Smirnov test.

(I) Integrins were activated using primary antibody followed by cross-linking Fab2 in HMDMs. Alexa-647-conjugated oxLDL binding was assessed and quantified as in (H).

*$p < 0.05$ was determined by the Kolmogorov-Smirnov test. See also Figure S5.

each increased lipid droplet formation by 1.54-, 2.28-, and 1.77-fold, respectively, when compared to controls incubated with oxLDL alone ($p < 0.05$, Figures 7A and 7B). Note that in the absence of oxLDL, the chemokines had little effect on lipid droplet formation, suggesting that they were not simply altering macrophage metabolism (Figure 7B). We additionally measured esterified cholesterol content by biochemical means. As shown in Figure S5E, in this assay CX_3CL1 increased the content of esterified cholesterol by 2.01-fold compared to controls, confirming the reliability of the BODIPY measurements ($p < 0.001$). These observations demonstrate that, by promoting engagement of oxLDL, chemokine signaling accelerates macrophage foam cell formation.

DISCUSSION

Our data demonstrate that by regulating the cortical actin cytoskeleton, integrin signaling exerts feedforward control over the

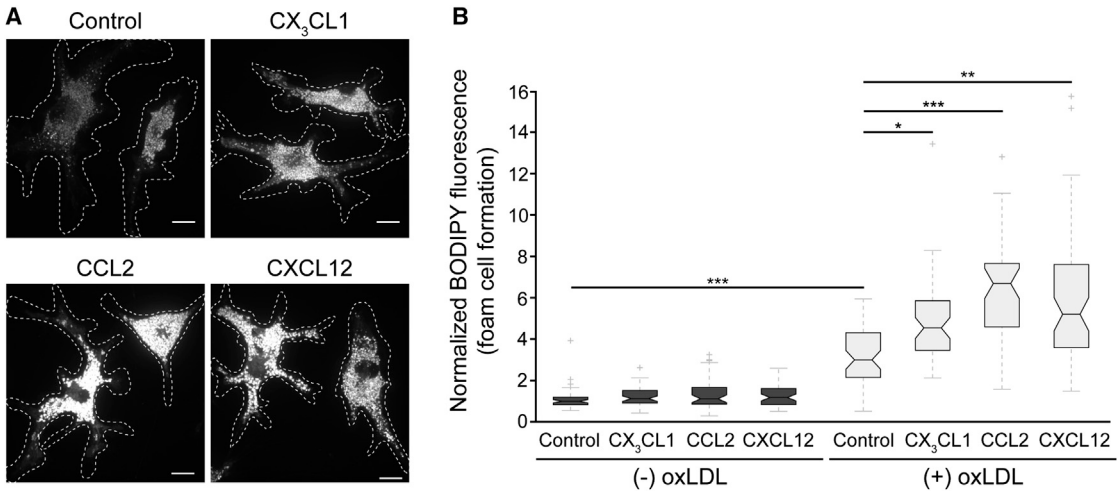

Figure 7. Chemokines Enhance Macrophage Foam Cell Formation

(A) BMDMs were incubated with 10% lipoprotein-deficient serum in the presence of CX_3CL1, CCL2, or CXCL12, and high concentrations of oxLDL for 24 hr. Lipid droplets were labeled with non-polar BODIPY. Representative extended focus z projections were obtained using spinning-disk confocal microscopy. Scale bars, 10 μm.

(B) Quantification of (A). The integrated BODIPY fluorescence was quantified per cell and normalized to control (–) oxLDL.

Data are from three independent experiments, each with ≥20 cells. Boxplots are as in Figure 1B. *$p < 0.05$, ***$p < 0.0001$ were determined by the Kruskal-Wallis test using Dunn's multiple comparisons test.

lateral diffusion and clustering of CD36 and, hence, the ability of macrophages to engage oxLDL. The degree of integrin engagement can be enhanced by chemokines, such as CX_3CL1, by promoting Rap1-mediated, inside-out activation. The resulting outside-in integrin signaling generates a highly dynamic cortical actin cytoskeleton, comprising actin-rich ruffles and adjacent actin-poor zones; the latter facilitates receptor clustering and serves as the predominant sites of oxLDL engagement. This, in turn, contributes to the increased accumulation of esterified cholesterol, accelerating macrophage foam cell formation. To the best of our knowledge, this is first demonstration that CD36 activity can be regulated through a mechanism other than cell-surface expression.

The notion of pre-clustering receptors independent of ligand is not unique to CD36. This phenomenon has been observed for immunoreceptors such as the T cell receptor (TCR), B cell receptor (BCR), and the high-affinity IgE receptor, FcεRI (Lillemeier et al., 2010; Mattila et al., 2013; Wilson et al., 2000). In the case of T lymphocytes, enhanced pre-clustering of the TCR in memory versus naive cells was reported to increase sensitivity to multivalent antigen by 100- to 3,000-fold. This effect is attributed in part to increased avidity for antigen arising from the increased multivalency of TCR oligomers (Kumar et al., 2011). A similar model has been proposed for the BCR (Fiala et al., 2013). In view of these studies and our own data, we propose that increased pre-clustering of CD36 in response to chemokines enhances its avidity for oxLDL. In addition, the enhanced clustering of CD36 may increase the rate of ligand rebinding and therefore reduce the effective dissociation constant of oxLDL. This concept is supported by studies utilizing computational modeling to investigate receptor-ligand interaction kinetics (Gopalakrishnan et al., 2005). Importantly, the effect of pre-clustering on ligand engagement will be highly dependent on the cell-surface density of the receptor, the rate at which clusters assemble and disassemble, as well as the concentration and multivalency of the ligand itself. It remains to be determined whether CD36 clusters are formed by homotypic interactions, as is the case for the TCR, or interactions with ancillary scaffolding molecules.

In our experimental setup, integrins bind substratum exclusively on the ventral cell surface and receptors bind oxLDL primarily on the dorsal cell surface. It is noteworthy that, in this system, integrin-mediated adhesion affects the cortical actin architecture not only at the ventral surface, but also at the dorsal surface. This effect is similar to what has been reported by Jaumouillé et al. (2014) and further demonstrates that integrin signaling controls both local and distal actin polymerization. While an informative model, the same scenario is unlikely to exist within the tissue microenvironment in vivo. Rather, extracellular matrix (ECM) will surround the cells in three-dimensional space, and a clear distinction between the dorsal and ventral membrane may not exist. The ECM, however, can be both compositionally and topographically heterogeneous in any given tissue and therefore integrins will not be engaged uniformly (Kubow and Horwitz, 2011). As a result, regions of the cortical cytoskeleton will by highly dynamic, similar to our in vitro system, creating "hot spots" of clustered CD36 distal to the sites of integrin engagement. The net effect of this response would be increased binding of oxLDL to spatially coordinated regions of the plasma membrane.

Apart from chemokines and other cytokines that activate integrins, the intrinsic mechanical properties of the ECM itself will also influence how prepared a macrophage is to engage oxLDL. These factors will dictate the degree of integrin activation, the type of integrin activated, and the resulting actin cytoskeletal architecture of a cell (Humphrey et al., 2014). It is important to note that the composition of the ECM is drastically altered as atherosclerotic lesions progress. The evolving ECM results from an

ever-changing cytokine milieu that drives vascular fibrosis, the deposition of transitional ECM components (i.e., fibronectin and fibrinogen), and the release of matrix-degrading enzymes (Akyildiz et al., 2014). Therefore, as atherogenesis proceeds, the ECM may be altered to a state that ''over-primes'' receptors to engage oxLDL. This notion is supported by our observations demonstrating that macrophages plated on integrin ligands have a higher degree of CD36 clustering, and a higher degree of oxLDL engagement compared to cells on substrates that limit integrin activation (Figure 6). Compositional changes will, in turn, affect the mechanical properties of the ECM such as rigidity, elasticity, as well as compressive and tensile strength, altering the amount of force exerted on individual macrophages (DuFort et al., 2011). These changes in forces are sensed and transduced primarily by integrins, which form a critical link between the ECM and the cytoskeleton. Thus, cells will respond to changes in mechanical force by adjusting their actin cytoskeletal architecture, thereby impacting CD36 clustering.

Our work highlights an unappreciated consequence of dysregulated chemokine production during atherogenesis: the continued priming of integrins by multiple chemokines will drive excessive engagement and internalization of oxLDL. During vascular inflammation, chemokines are traditionally thought to promote the recruitment of leukocytes to the vascular wall. However, it is becoming increasingly apparent that they can additionally impact immune function directly (Zernecke and Weber, 2010). The priming of receptors for engagement of oxLDL can now be included in the list of effects elicited by the chemokines. Thus, it is conceivable that a detrimental feedback loop results following initial macrophage recruitment to the intima; cells over-activate integrins in response to dysregulated chemokine production and thereby excessively prime receptors. As a result, the macrophages accumulate oxLDL, transform into foam cells, undergo necrosis, and subsequently release pro-inflammatory stimuli that exacerbate production of more chemokines. During atherogenesis in vivo, it is likely that multiple chemokines exert synergistic effects and that their collective inputs dictate the integrated macrophage response (e.g., CD36 clustering) and the progression of atherosclerosis. Two lines of evidence support this notion: (1) three structurally distinct chemokines that we tested each enhanced CD36 clustering, the engagement of oxLDL, and the accumulation of esterified cholesterol and (2) triple deletion of CX_3CR1, CCR5, and CCL2 in $ApoE^{-/-}$ mice yields an additive reduction in atherosclerosis (Combadière et al., 2008).

Overall, our data suggest that receptor clustering may serve as a tunable variable, controlled by the integration of cytokine inputs that converge on integrin signaling, and ultimately influence the progression of inflammation.

EXPERIMENTAL PROCEDURES

OxLDL Binding and Internalization

OxLDL internalization was assessed in macrophages incubated with DiI oxLDL for 25 min at 37° in the presence or absence of CX_3CL1 (100 ng/ml), followed by washing with PBS. Prior to fixation, non-internalized oxLDL was removed by a 1-min incubation with trypsin. For binding assays, macrophages were pre-treated with CX_3CL1 (100 ng/ml) for 5 min at 37°C. OxLDL binding was assessed by incubating cells with either DiI oxLDL (2 μg/ml) or Alexa-647-conjugated oxLDL (2 μg/ml) for 1 min at 37°, followed by washing with PBS and fixation. OxLDL fluorescence per cell was measured using ImageJ software as described in Image Processing and Analysis (see Supplemental Experimental Procedures). All animal experiments were approved by The Hospital for Sick Children Institutional Animal Care and Use Committee, and adhered to the NIH Guide for the Care and Use of Laboratory Animals.

Single-Molecule Imaging and Diffusion Analysis

Cells were initially blocked with 5% donkey serum for 5 min and incubated with anti-CD36 Fab fragment (clone 131.1) diluted in HEPES-buffered RPMI-1640 (HPMI). Following washing, cells were incubated with biotin-conjugated secondary Fab fragment (0.375 μg/ml) diluted in HPMI for 10 min. In the latter case, cells were washed further then incubated with Qdot 655-conjugated-streptavidin (0.1 nM) diluted in biotin-free HBSS for 4 min. Unengaged streptavidin was blocked by brief incubation with HPMI containing 0.2 μg/ml biotin, followed by washing. All labeling steps and washes were performed at 10°C to minimize receptor cross-linking. Coverslips were transferred to Leiden chambers, incubated in HPMI, and warmed to 37°C for live imaging.

For CD36 clustering analysis, cells were fixed in 4% paraformaldehyde (PFA) for 20 min, and labeling was performed as described above using anti-CD36 Fab fragment and secondary anti-mouse Cy3-conjugated Fab fragment (0.750 μg/ml). Cells were post-fixed using 3% PFA supplemented with 0.1% gluteraldehyde for 10 min. For each fixation step, excess aldehydes were neutralized with 100 mM glycine.

Single-molecule tracking was performed using a Carl Zeiss Axiovert 200 M inverted epifluorescence microscope equipped with a heated stage, a custom 2.5× magnifying lens, a 100× (numerical aperture [NA] 1.45) oil-immersion objective, an Exfo X-Cite 120 light source, and a Hamamatsu C9100-13 back-thinned, electron-multiplying charge-coupled device (EM-CCD) camera. Images were acquired on the dorsal cell surface at a frame rate of 33 Hz for Qdots using Volocity software (PerkinElmer).

Single molecules were detected and tracked as described previously for CD36 (Jaqaman et al., 2008, 2011). Motion classifications and diffusion coefficients were determined using a moment scaling spectrum (MSS) analysis (Ewers et al., 2005; Ferrari et al., 2001; Jaqaman et al., 2011). Confinement dimensions were derived by eigenvalue decomposition of the variance-covariance matrix of particle positions (Jaqaman et al., 2011).

In some instances, adherent macrophages were lifted into suspension using 10 mM EDTA and dropped onto coverslips coated with 5% BSA, fibronectin (50 μg/ml) or collagen IV (50 μg/ml) for 30 min. Cells were then labeled for single-molecule tracking and imaged as described above.

Spinning-Disk Confocal Microscopy

The spinning-disk confocal system (Quorum Technologies) consisted of an Axiovert 200 M microscope (Carl Zeiss) equipped with a 63× (NA 1.4) oil immersion objective as well an additional 1.5× magnifying lens. This microscope was equipped with diode-pumped solid-state lasers (440, 491, 561, 638, and 655 nm; Spectral Applied Research) and a motorized XY stage (Applied Scientific Instrumentation). Images were acquired using a back-thinned, EM-CCD camera (model C9100-13 ImagEM; Hamamatsu Photonics) controlled using Volocity software, v.6.0.1 (PerkinElmer).

Structured Illumination Microscopy

Fixed samples were mounted using Prolong Diamond Antifade Mountant (Life Technologies). Images were acquired using the Carl Zeiss ELYRA PS1 system equipped with an Axio Observer Z1 microscope, a 63× (1.4 NA) apochromat oil immersion objective, a 1.6× optovar, and an Andor iXon3 885 EM-CCD camera. Three orientation angles of the excitation grid with five phases each were acquired for each z plane. Images were reconstructed using the structured illumination module included with the ZEN software package (Carl Zeiss).

SUPPLEMENTAL INFORMATION

Supplemental Information includes Supplemental Experimental Procedures and five figures and can be found with this article online at http://dx.doi.org/10.1016/j.celrep.2016.02.071.

AUTHOR CONTRIBUTIONS

H.S.W. designed and performed experiments, analyzed and interpreted the data, and prepared the manuscript. V.J. and S.A.F. designed experiments and edited the manuscript. S.A.D. and D.S. performed and assisted with key experiments. J.C. assisted with HMDM and BMDM preparation and performed flow cytometry. I.M.M. and A.S. assisted with HMDM and BMDM preparations, respectively. S.G. and L.A.R. designed experiments, interpreted data, and prepared the manuscript.

ACKNOWLEDGMENTS

We would like to thank Paul Paroutis from the SickKids imaging facility for assistance with image analysis. H.S.W. is supported by Restracomp from the Hospital for Sick Children. S.A.F. is supported by a fellowship from the Heart and Stroke Foundation of Canada. L.A.R. is a Canada Research Chair (Tier 2). This work was funded by grants from the Natural Sciences and Engineering Research Council of Canada DGPIN 418496-12 and from the Canadian Institutes for Health Research MOP-7075.

Received: August 31, 2015
Revised: December 22, 2015
Accepted: February 16, 2016
Published: March 17, 2016

REFERENCES

Abram, C.L., and Lowell, C.A. (2009). The ins and outs of leukocyte integrin signaling. Annu. Rev. Immunol. *27*, 339–362.

Akyildiz, A.C., Speelman, L., and Gijsen, F.J. (2014). Mechanical properties of human atherosclerotic intima tissue. J. Biomech. *47*, 773–783.

Andrews, N.L., Lidke, K.A., Pfeiffer, J.R., Burns, A.R., Wilson, B.S., Oliver, J.M., and Lidke, D.S. (2008). Actin restricts FcepsilonRI diffusion and facilitates antigen-induced receptor immobilization. Nat. Cell Biol. *10*, 955–963.

Bezbradica, J.S., Rosenstein, R.K., DeMarco, R.A., Brodsky, I., and Medzhitov, R. (2014). A role for the ITAM signaling module in specifying cytokine-receptor functions. Nat. Immunol. *15*, 333–342.

Boring, L., Gosling, J., Cleary, M., and Charo, I.F. (1998). Decreased lesion formation in CCR2-/- mice reveals a role for chemokines in the initiation of atherosclerosis. Nature *394*, 894–897.

Caron, E., Self, A.J., and Hall, A. (2000). The GTPase Rap1 controls functional activation of macrophage integrin alphaMbeta2 by LPS and other inflammatory mediators. Curr. Biol. *10*, 974–978.

Combadière, C., Potteaux, S., Rodero, M., Simon, T., Pezard, A., Esposito, B., Merval, R., Proudfoot, A., Tedgui, A., and Mallat, Z. (2008). Combined inhibition of CCL2, CX3CR1, and CCR5 abrogates Ly6C(hi) and Ly6C(lo) monocytosis and almost abolishes atherosclerosis in hypercholesterolemic mice. Circulation *117*, 1649–1657.

del Pozo, M.A., Alderson, N.B., Kiosses, W.B., Chiang, H.H., Anderson, R.G., and Schwartz, M.A. (2004). Integrins regulate Rac targeting by internalization of membrane domains. Science *303*, 839–842.

DuFort, C.C., Paszek, M.J., and Weaver, V.M. (2011). Balancing forces: architectural control of mechanotransduction. Nat. Rev. Mol. Cell Biol. *12*, 308–319.

Endemann, G., Stanton, L.W., Madden, K.S., Bryant, C.M., White, R.T., and Protter, A.A. (1993). CD36 is a receptor for oxidized low density lipoprotein. J. Biol. Chem. *268*, 11811–11816.

Ewers, H., Smith, A.E., Sbalzarini, I.F., Lilie, H., Koumoutsakos, P., and Helenius, A. (2005). Single-particle tracking of murine polyoma virus-like particles on live cells and artificial membranes. Proc. Natl. Acad. Sci. USA *102*, 15110–15115.

Febbraio, M., Podrez, E.A., Smith, J.D., Hajjar, D.P., Hazen, S.L., Hoff, H.F., Sharma, K., and Silverstein, R.L. (2000). Targeted disruption of the class B scavenger receptor CD36 protects against atherosclerotic lesion development in mice. J. Clin. Invest. *105*, 1049–1056.

Ferrari, R., Manfroi, A.J., and Young, W.R. (2001). Strongly and weakly self-similar diffusion. Physica D *104*, 111–137.

Fiala, G.J., Kaschek, D., Blumenthal, B., Reth, M., Timmer, J., and Schamel, W.W. (2013). Pre-clustering of the B cell antigen receptor demonstrated by mathematically extended electron microscopy. Front. Immunol. *4*, 427.

Flannagan, R.S., Harrison, R.E., Yip, C.M., Jaqaman, K., and Grinstein, S. (2010). Dynamic macrophage "probing" is required for the efficient capture of phagocytic targets. J. Cell Biol. *191*, 1205–1218.

Freeman, S.A., and Grinstein, S. (2014). Phagocytosis: receptors, signal integration, and the cytoskeleton. Immunol. Rev. *262*, 193–215.

Freeman, S.A., Jaumouillé, V., Choi, K., Hsu, B.E., Wong, H.S., Abraham, L., Graves, M.L., Coombs, D., Roskelley, C.D., Das, R., et al. (2015). Toll-like receptor ligands sensitize B-cell receptor signalling by reducing actin-dependent spatial confinement of the receptor. Nat. Commun. *6*, 6168.

Gevrey, J.C., Isaac, B.M., and Cox, D. (2005). Syk is required for monocyte/macrophage chemotaxis to CX3CL1 (Fractalkine). J. Immunol. *175*, 3737–3745.

Gopalakrishnan, M., Forsten-Williams, K., Nugent, M.A., and Täuber, U.C. (2005). Effects of receptor clustering on ligand dissociation kinetics: theory and simulations. Biophys. J. *89*, 3686–3700.

Humphrey, J.D., Dufresne, E.R., and Schwartz, M.A. (2014). Mechanotransduction and extracellular matrix homeostasis. Nat. Rev. Mol. Cell Biol. *15*, 802–812.

Jaqaman, K., Loerke, D., Mettlen, M., Kuwata, H., Grinstein, S., Schmid, S.L., and Danuser, G. (2008). Robust single-particle tracking in live-cell time-lapse sequences. Nat. Methods *5*, 695–702.

Jaqaman, K., Kuwata, H., Touret, N., Collins, R., Trimble, W.S., Danuser, G., and Grinstein, S. (2011). Cytoskeletal control of CD36 diffusion promotes its receptor and signaling function. Cell *146*, 593–606.

Jaumouillé, V., Farkash, Y., Jaqaman, K., Das, R., Lowell, C.A., and Grinstein, S. (2014). Actin cytoskeleton reorganization by Syk regulates Fcγ receptor responsiveness by increasing its lateral mobility and clustering. Dev. Cell *29*, 534–546.

Katagiri, K., Maeda, A., Shimonaka, M., and Kinashi, T. (2003). RAPL, a Rap1-binding molecule that mediates Rap1-induced adhesion through spatial regulation of LFA-1. Nat. Immunol. *4*, 741–748.

Kim, J.G., Moon, M.Y., Kim, H.J., Li, Y., Song, D.K., Kim, J.S., Lee, J.Y., Kim, J., Kim, S.C., and Park, J.B. (2012). Ras-related GTPases Rap1 and RhoA collectively induce the phagocytosis of serum-opsonized zymosan particles in macrophages. J. Biol. Chem. *287*, 5145–5155.

Kleemann, R., Zadelaar, S., and Kooistra, T. (2008). Cytokines and atherosclerosis: a comprehensive review of studies in mice. Cardiovasc. Res. *79*, 360–376.

Kubow, K.E., and Horwitz, A.R. (2011). Reducing background fluorescence reveals adhesions in 3D matrices. Nat. Cell Biol. *13*, 3–5, author reply 5–7.

Kumar, R., Ferez, M., Swamy, M., Arechaga, I., Rejas, M.T., Valpuesta, J.M., Schamel, W.W., Alarcon, B., and van Santen, H.M. (2011). Increased sensitivity of antigen-experienced T cells through the enrichment of oligomeric T cell receptor complexes. Immunity *35*, 375–387.

Kunjathoor, V.V., Febbraio, M., Podrez, E.A., Moore, K.J., Andersson, L., Koehn, S., Rhee, J.S., Silverstein, R., Hoff, H.F., and Freeman, M.W. (2002). Scavenger receptors class A-I/II and CD36 are the principal receptors responsible for the uptake of modified low density lipoprotein leading to lipid loading in macrophages. J. Biol. Chem. *277*, 49982–49988.

Kusumi, A., Nakada, C., Ritchie, K., Murase, K., Suzuki, K., Murakoshi, H., Kasai, R.S., Kondo, J., and Fujiwara, T. (2005). Paradigm shift of the plasma membrane concept from the two-dimensional continuum fluid to the partitioned fluid: high-speed single-molecule tracking of membrane molecules. Annu. Rev. Biophys. Biomol. Struct. *34*, 351–378.

Landsman, L., Bar-On, L., Zernecke, A., Kim, K.W., Krauthgamer, R., Shagdarsuren, E., Lira, S.A., Weissman, I.L., Weber, C., and Jung, S. (2009). CX3CR1 is required for monocyte homeostasis and atherogenesis by promoting cell survival. Blood *113*, 963–972.

Lillemeier, B.F., Mörtelmaier, M.A., Forstner, M.B., Huppa, J.B., Groves, J.T., and Davis, M.M. (2010). TCR and Lat are expressed on separate protein islands on T cell membranes and concatenate during activation. Nat. Immunol. *11*, 90–96.

Ma, W., Liu, Y., Ellison, N., and Shen, J. (2013). Induction of C-X-C chemokine receptor type 7 (CXCR7) switches stromal cell-derived factor-1 (SDF-1) signaling and phagocytic activity in macrophages linked to atherosclerosis. J. Biol. Chem. *288*, 15481–15494.

Mattila, P.K., Feest, C., Depoil, D., Treanor, B., Montaner, B., Otipoby, K.L., Carter, R., Justement, L.B., Bruckbauer, A., and Batista, F.D. (2013). The actin and tetraspanin networks organize receptor nanoclusters to regulate B cell receptor-mediated signaling. Immunity *38*, 461–474.

Murphy, D.A., and Courtneidge, S.A. (2011). The 'ins' and 'outs' of podosomes and invadopodia: characteristics, formation and function. Nat. Rev. Mol. Cell Biol. *12*, 413–426.

Nozaki, S., Kashiwagi, H., Yamashita, S., Nakagawa, T., Kostner, B., Tomiyama, Y., Nakata, A., Ishigami, M., Miyagawa, J., Kameda-Takemura, K., et al. (1995). Reduced uptake of oxidized low density lipoproteins in monocyte-derived macrophages from CD36-deficient subjects. J. Clin. Invest. *96*, 1859–1865.

Okigaki, M., Davis, C., Falasca, M., Harroch, S., Felsenfeld, D.P., Sheetz, M.P., and Schlessinger, J. (2003). Pyk2 regulates multiple signaling events crucial for macrophage morphology and migration. Proc. Natl. Acad. Sci. USA *100*, 10740–10745.

Park, H., and Cox, D. (2011). Syk regulates multiple signaling pathways leading to CX3CL1 chemotaxis in macrophages. J. Biol. Chem. *286*, 14762–14769.

Ridley, A.J., Paterson, H.F., Johnston, C.L., Diekmann, D., and Hall, A. (1992). The small GTP-binding protein rac regulates growth factor-induced membrane ruffling. Cell *70*, 401–410.

Seimon, T.A., Nadolski, M.J., Liao, X., Magallon, J., Nguyen, M., Feric, N.T., Koschinsky, M.L., Harkewicz, R., Witztum, J.L., Tsimikas, S., et al. (2010). Atherogenic lipids and lipoproteins trigger CD36-TLR2-dependent apoptosis in macrophages undergoing endoplasmic reticulum stress. Cell Metab. *12*, 467–482.

Sheedy, F.J., Grebe, A., Rayner, K.J., Kalantari, P., Ramkhelawon, B., Carpenter, S.B., Becker, C.E., Ediriweera, H.N., Mullick, A.E., Golenbock, D.T., et al. (2013). CD36 coordinates NLRP3 inflammasome activation by facilitating intracellular nucleation of soluble ligands into particulate ligands in sterile inflammation. Nat. Immunol. *14*, 812–820.

Stewart, C.R., Stuart, L.M., Wilkinson, K., van Gils, J.M., Deng, J., Halle, A., Rayner, K.J., Boyer, L., Zhong, R., Frazier, W.A., et al. (2010). CD36 ligands promote sterile inflammation through assembly of a Toll-like receptor 4 and 6 heterodimer. Nat. Immunol. *11*, 155–161.

Tabas, I., Williams, K.J., and Borén, J. (2007). Subendothelial lipoprotein retention as the initiating process in atherosclerosis: update and therapeutic implications. Circulation *116*, 1832–1844.

Wells, C.M., Walmsley, M., Ooi, S., Tybulewicz, V., and Ridley, A.J. (2004). Rac1-deficient macrophages exhibit defects in cell spreading and membrane ruffling but not migration. J. Cell Sci. *117*, 1259–1268.

Williams, K.J., and Tabas, I. (1999). Atherosclerosis–an inflammatory disease. N. Engl. J. Med. *340*, 1928, author reply 1929.

Wilson, B.S., Pfeiffer, J.R., and Oliver, J.M. (2000). Observing FcepsilonRI signaling from the inside of the mast cell membrane. J. Cell Biol. *149*, 1131–1142.

Yi, L., Chandrasekaran, P., and Venkatesan, S. (2012). TLR signaling paralyzes monocyte chemotaxis through synergized effects of p38 MAPK and global Rap-1 activation. PLoS ONE *7*, e30404.

Zernecke, A., and Weber, C. (2010). Chemokines in the vascular inflammatory response of atherosclerosis. Cardiovasc. Res. *86*, 192–201.

Zernecke, A., and Weber, C. (2014). Chemokines in atherosclerosis: proceedings resumed. Arterioscler. Thromb. Vasc. Biol. *34*, 742–750.